Arab J Geosci (2017) 10: 175
DOI 10.1007/s12517-017-2972-6

ORIGINAL PAPER

Geological mapping of Santorini Volcanic island (Greece), with the combined use of Pleiades 1A and ENVISAT satellite images

Dimitrios Oikonomidis[1] · **Spyridon Pavlides**[1]

Received: 27 May 2016 / Accepted: 27 March 2017 / Published online: 4 April 2017

Abstract Very high-resolution (VHR) Pleiades 1A and ENVISAT/ASAR (Advanced Synthetic Aperture Radar) satellite images were used for lithological and tectonic mapping respectively of Santorini island complex, South Aegean, Greece. The results were compared to the existing geological maps of the study area. The extracted, quantitative results within GIS environment, followed by a ground-truth visit, showed that there is some variance in the delineation of the boundaries of certain lithological units on the geological map compared to those on the Pleiades 1A image and that a number of lineaments detected on the ENVISAT image could be incorporated to the faults' population. As a general conclusion, new findings can be embodied to the existing geological maps.

Keywords Pleiades · ENVISAT · Lithological mapping · Lineaments

Introduction

Santorini island complex consists of the main island of Thera covering an area of 75.92 km^2, Therasia (9.19 km^2), Palea Kammeni (0.51 km^2), Nea Kammeni where the active volcano is located (3.33 km^2) and Aspronisi (0.12 km^2). It is located at the southern Aegean (Fig. 1). It consists of a variety of volcanic rocks, mainly pumice and lavas. The oldest rocks of the Santorini island complex are the metamorphic formation (mainly limestones) covering a small area at the SE part of Thera (Upper Triassic to Eocene), while the volcanic rocks of various explosive activity are dated as back as 2 Ma up to present period (1950 AD). The area belongs to the Mediterranean climate type and a considerable part is covered by agricultural land (mainly vineyards). The island is also famous for its big caldera (approximately 10 km long in the N-S direction and 6.5 km in the E-W direction), which was formed after the devastating eruption of 1613 (±13) BC (Friedrich et al. 2006).

Remotely sensed images have been increasingly used for the creation and updating of geological maps since the launch of Landsat-1 in 1972. A variety of image processing and analysis techniques have been developed for the extraction and delineation of lithological boundaries out of satellite imagery (Behnia et al. 2012; Hadigheh and Ranjbar 2013; He et al. 2015; Jakob et al. 2015; Othman and Gloaguen 2014; Pour and Hashim 2015a; Puornamdari et al. 2014; Rowan and Mars 2003; Yamaguchi and Naito 2009; Zhang and Li 2014). However, all the research that has been performed till today, work on arid or semiarid places of the Earth, where rocks are well-exposed, or they concern with the mapping of a single rock or similar rock types. In the present study, lithological boundaries of very similar rock types could be mapped (namely varieties of pumice and lavas with subtle differences), due to the spectral and spatial properties of high-quality Pleiades imagery that allowed to overcome the drawback of the vegetation, where present.

Complementary to the above, geologists have used mainly radar spaceborne Synthetic Aperture Radar/SAR images to define structural geological trends that is to draw lineaments as structural indicators (Arlegui and Soriano 2003; Bogdanov et al. 2011; Liu et al. 2010; Morelli and Piana 2006; Pal et al.

✉ Dimitrios Oikonomidis
oikonomi@geo.auth.gr

Spyridon Pavlides
pavlides@geo.auth.gr

[1] School of Geology, Aristotle University of Thessaloniki, 54124 Thessaloniki, Greece

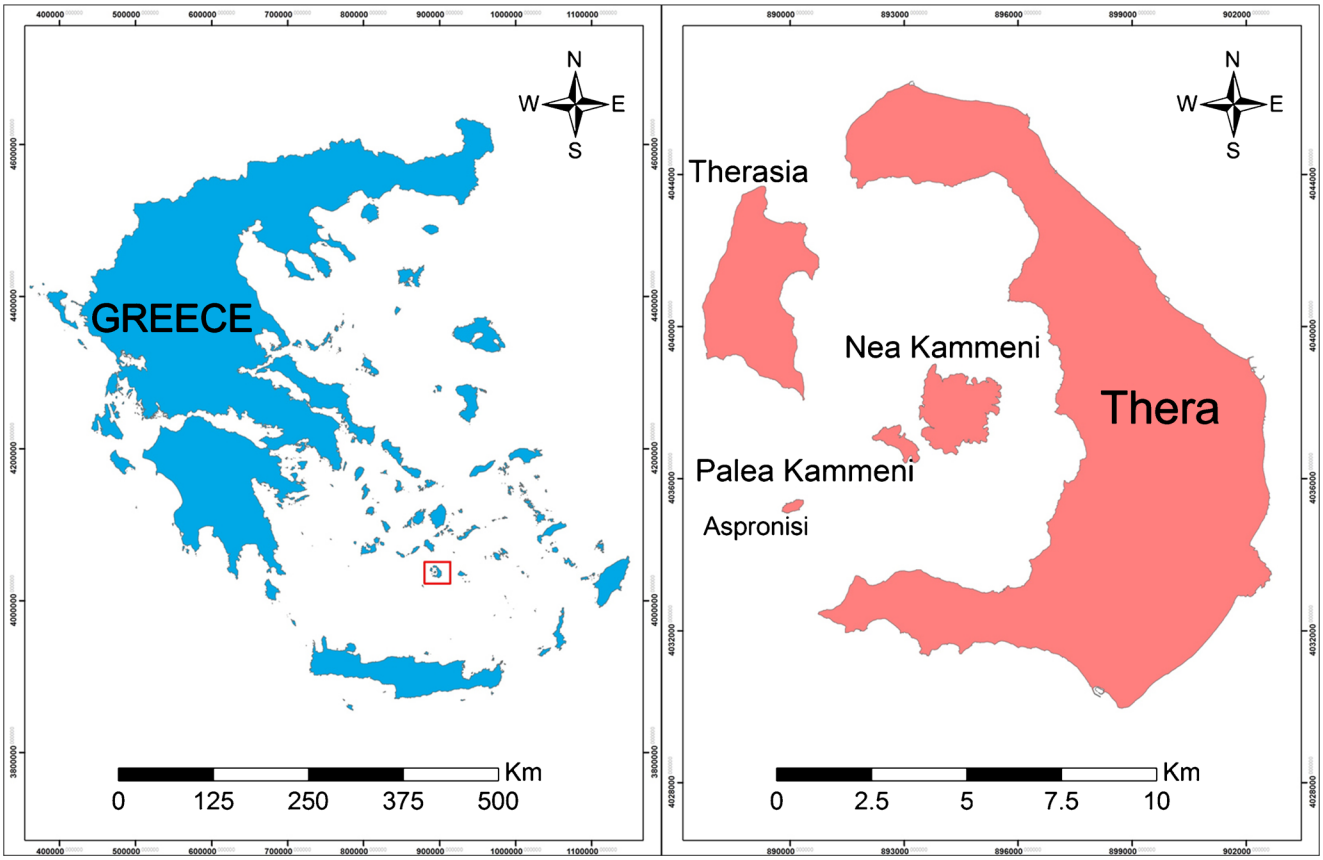

Fig. 1 Location of Santorini study area

Table 1 Available data and software

Available data and software	Technical characteristics
Geological map (1)	Geological map of the Santorini islands of 1/20.000 scale. Source: Druitt et al. (1999).
Geological map (2)	Geological map of the Santorini islands of 1/50.000 scale. Source: IGME (Institute of Geological and Mineral Exploration)/1980.
Geological map (3)	The Neotectonic map of the Santorini islands. Source: Conference Paper by Mountrakis et al. (1998).
Satellite image (1)	3 Pleiades 1A satellite images, kindly provided by Airbus Defence and Space (ordered via Geostore), through ESA's Category-1 current Project. Each image contains 4 multispectral bands (blue, green red and NIR) and 1 panchromatic band with spatial resolutions 2 and 0.5 m, respectively (http://www.geo-airbusds.com/en/3027-pleiades-50-cm-resolution-products). 1) ID:DS_PHR1A_201306080901112_FR1_PX_E025N36_0512_00301 Date Acquired: 2013/06/08. 2) ID:DS_PHR1A_201306080901107_FR1_PX_E025N36_0412_0049 7. Date Acquired: 2013/06/08. 3) ID:DS_PHR1A_201306080901103_FR1_PX_E025N36_0611_0124 8. Date Acquired: 2013/06/08.
Satellite image (2)	1 (one) ENVISAT/ASAR radar satellite image at C-Band, kindly provided by the European Space Agency/ESA through the current Category-1 Project. ID:ASA_IMG_1PNUPA20050128_082853_000000162034_00150_15,234_0554.N1 Date acquired: 2005/01/28. Pass: Descending. Track: 150. Orbit: 15,234. Type: ASA_IMG_1P. Spatial resolution: Initially 25 m, provided at 12.5 m pixel size.
Software (1)	Software for GIS: ArcGIS v.10.2.2
Software (2)	Software for digital processing of the Pleiades and ENVISAT satellite imagery: ENVI v.5.1
Software (3)	Software for processing the ENVISAT imagery: ESA's Sentinel-1 Toolbox.

2007; Pour and Hashim 2015b; Prieto et al. 2015; Saadi and Watanabe 2009). According to O'Leary et al. (1976), a lineament is defined as "a mappable, simple or composite linear feature of a surface, whose parts are aligned in a rectilinear or slightly curvilinear relationship and which differs distinctly from the patterns of adjacent features and presumably reflects a subsurface phenomenon". Lineaments, which may be continuous or discontinuous, may be considered as the surface display of fault and fracture zones. Lineaments can be very clearly surveyed on SAR images due to the competence of the radar microwave beam to penetrate clouds, rain, snow and vegetation and therefore reach the underlying terrain and

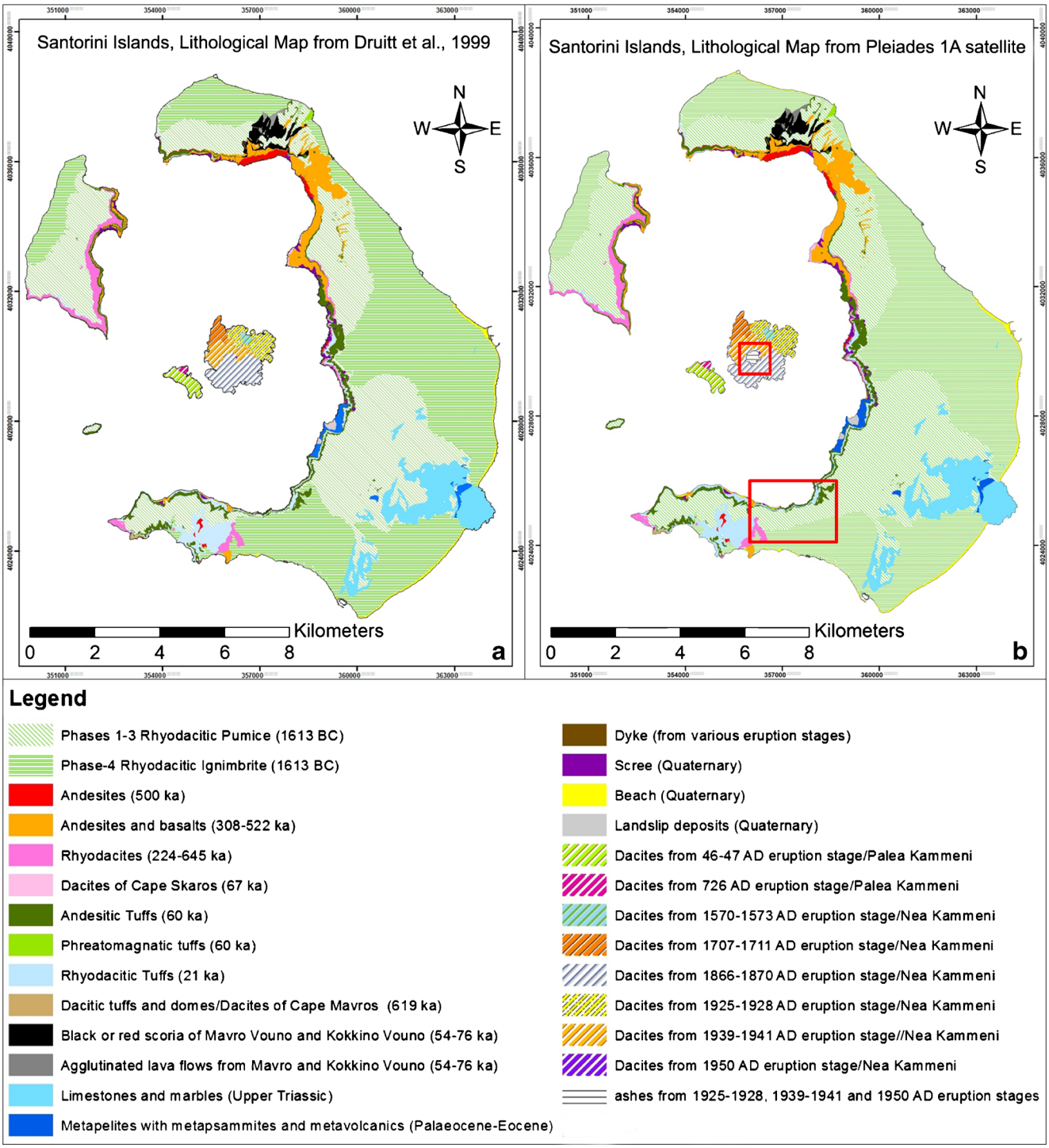

Fig. 2 Lithological mapping of Santorini islands after the geological map of Druitt et al., 1999 (**2a**) and Pleiades 1a images (**2b**). Rock boundaries in (**2a**) simplified by the authors. Modified areas within *red rectangles*

delineate its discontinuities (European Space Agency/ESA 2005). In many cases, structural features, such as faults, fractures, folds etc. have been detected, as well as extended.

The objective of this study is multidimensional: firstly, to carry out lithological mapping of Santorini island complex, which consists of successive layers of volcanic rocks and is a partly-vegetated terrain, using VHR Pleiades 1A satellite imagery, and secondly, to access the utilization of ENVISAT/ASAR radar imagery for structural mapping and finally to compare the above quantitative results to the geological data provided by the geological map of the area of Druitt et al. 1999.

Data collection

The following data and software were used in the present study (Table 1):

All the above data were projected in UTM/Zone 35N, Datum: WGS84 and have been entered to a geographical information system/GIS environment.

ENVISAT/ASAR image acquisition date is not of highest importance since radar images are recorded without atmospheric interference due to the microwave beam properties, so the selection of the specific image had to do only with the fact that in that date, Santorini island complex was depicted in a single frame and not in two or more frames as in other acquisition dates. On the other hand, the absence of any kind of atmospheric precipitation or clouds was the criterion to select the acquisition date of the Pleiades optical imagery.

Processing and results

Geology

Santorini is one of the largest Quaternary volcanic centres. The caldera rocks show sequences of lavas and pyroclastic deposits that were deposited in the past. They are the products of 12 major explosive eruptions and the dissected remains of several ancient lava fields, stratovolcanoes and lava-dome complexes. The existence of numerous eruptive centres shows that Santorini islands can be better described as a volcanic field. The repeated explosive eruptions created the formation of four large calderas in the past, the present-day caldera being the fourth one. Santorini is potentially one of the most dangerous volcanoes in Europe, having had numerous eruptions in historic times (Druitt et al. 1999).

Santorini islands were built on a pre-volcanic island of metamorphic rocks (metapelites and limestones marbles) which were formed in a period from Upper Triassic to Palaeocene-Eocene.

The early volcanic centres of Akrotiri Peninsula (southern Thera) date back to 650–550 ka, followed by the so-called Peristeria Volcano (530–430 ka) and the cinder cones of the Akrotiri Peninsula (southern Thera, 450–340 ka). Then the first and second explosive cycles took place (c. 360–180 ka and 180–3.6 ka, respectively), before the vast eruption of the late Bronze Age (c. 3.6 ka or 1613 BC) which formed the present-day caldera. As a result of this, Thera, Therasia and Aspronisi are covered by a layer of white tuff (phases 1–4, mainly pumice). After a long time of being dormant, the volcano "woke up" again in historical times, forming the dacite-consisted islands of Palea Kammeni and Nea Kammeni inside the caldera (46–1950 AD). The present-day volcanic centres are located on the island of Nea Kammeni.

The most recent geological map of Santorini islands by Druitt et al. (1999) was scanned and georeferenced, the boundaries of lithological formations were digitized and the areas of lithological formations were calculated within ArcMap v. 10.2.2 environment (Fig. 2 a and Table 2).

Table 2 Areas of lithological formations from the geological map of Fig. 2

Rock	Area (km^2)
Phases 1–3 rhyodacitic pumice	29.06
Phase 4 rhyodacitic ignimbrite	37.97
Andesites	0.42
Andesites and basalts	3.16
Rhyodacites	1.62
Dacites of Cape Skaros	0.07
Andesitic tuffs	2.76
Phreatomagmatic tuffs	0.06
Rhyodacitic tuffs	2.31
Dacitic phreatomagmatic tuffs and domes/dacites of Cape Mavros	0.04
Black or red Scoria of Mavro Vouno and Kokkino Vouno	0.89
Agglutinated spatter and clastogenic lava flows from Mavro Vouno and Kokkino Vouno	0.14
Limestones and marbles	4.84
Metapelites with metapsammites, metavolcanics and marbles	0.54
Dyke	0.05
Scree	0.51
Beach	0.70
Landslip deposits	0.10
Dacites 46–47/Palea Kammeni	0.46
Dakites 726/Palea Kammeni	0.05
Dakites 1570–1573/Nea Kammeni	0.09
Dacites 1707–1711/Nea Kammeni	0.33
Dacites 1866–1870/Nea Kammeni	1.42
Dacites 1925–1928/Nea Kammeni	0.83
Dacites 1939–1941/Nea Kammeni	0.65
Dacites 1950/Nea Kammeni	0.01

Pleiades 1A

The initial three Pleiades 1A images covering Santorini islands were mosaicked into a single multispectral and a single panchromatic file, followed by atmospheric and radiometric corrections and image pan-sharpening. Various digital image processing techniques were used in order to determine the image that would best map the lithological formations of the island, such as spectral angle mapper, spectral feature filtering, matched filtering and linear band prediction (LS-Fit). The above techniques did not depict the known rocks with satisfactory accuracy. This happened because these methodologies use reference spectra from powdered, pure rocks to be matched with the image spectra (pixel values of out-door rocks). In our case, the pixel values are the outcome of component reflectivities, resulting from both rock outcrops and vegetation, so these methodologies could not yield working results. Therefore, the ultimate solution was to create a false colour composite (FCC) for visual interpretation.

For this purpose, reflectance values of the most widespread rock type which is pumice (phases 1–4 in the geological map legend of Fig. 2) was studied with the help of the Jet Propulsion Laboratory/JPL spectral library, embodied in ENVI software. Pumice shows relatively high reflectance values in the spectrum of band 4 of Pleiades 1A satellite image and lower values in bands 2 and 1, therefore in the 4,2,1:RGB FCC image, pumice appears in a brown-reddish colour and in the 1,4,PC4 RGB FCC image the same rock appears in green colour. Other rocks of the Santorini island complex are well distinguished in the aforementioned FCC images. PC4 stands for principal component 4 band, resulting from principal component analysis technique. A histogram equalization and a linear stretch were applied on the above FCCs respectively to enhance their appearance (Fig. 3).

After that, a supervised classification technique, using a maximum likelihood classifier was applied in the above FCC images, the results being poor due to significant spectral overlap percentage of the classes that typify the volcanic rocks of the islands. Therefore, the above FCC images were imported to ArcMap where they were used as background images in order to manually digitize the boundaries of the lithological formations based on the authors' good geological

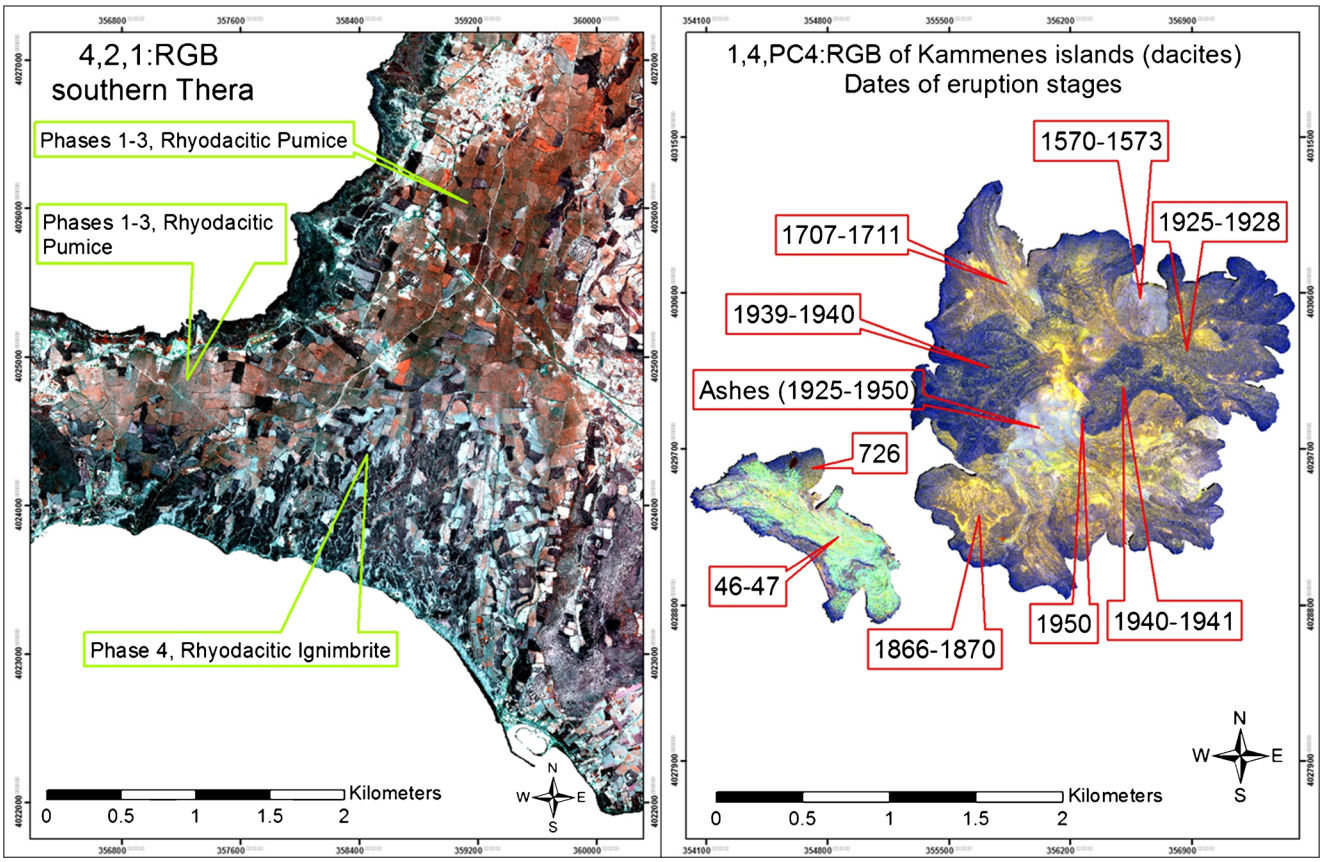

Fig. 3 **3a**/left: 4,2,1:RGB FCC image of southern Thera island. Discrimination between Phases 1–3 (rhyodacitic pumice) and Phase 4 (rhyodacitic ignimbrite) of the 1613 ± 13 BC eruption. *3b*/right: 1,4,PC4:RGB FCC image of the Kammenes islands (Palea Kammeni on the left and Nea Kammeni on the right), at the centre of the Santorini caldera. The dacites lavas of different eruption dates as well as a thin ash layer, can be clearly recognized

knowledge of the area (Fig. 2 b). The areas measured for each formation are shown in Table 3.

ENVISAT/ASAR

SAR images have inherent "salt and pepper"-like texturing called speckles which degrade the quality of the image and make interpretation of features more difficult. Speckles are caused by random constructive and destructive interference of the de-phased but coherent return waves scattered by the elementary scatters within each resolution cell. Speckle noise reduction can be applied either by spatial filtering or multilook processing. In our case, a de-speckle technique was applied, using the refined Lee filter, with a threshold of 5000. Then, the sea was masked out of the ENVISAT/ASAR image in order to keep only the land areas.

Table 3 Areas of lithological formations derived from the Pleiades-1A satellite imagery

Rock	Area (km^2)
Phases 1–3 rhyodacitic pumice	30.83
Phase 4 rhyodacitic ignimbrite	36.20
Andesites	0.42
Andesites and basalts	3.16
Rhyodacites	1.62
Dacites of Cape Skaros	0.07
Andesitic tuffs	2.76
Phreatomagmatic tuffs	0.06
Rhyodacitic tuffs	2.31
Dacitic phreatomagmatic tuffs and domes/dacites of Cape Mavros	0.04
Black or red Scoria of Mavro Vouno and Kokkino Vouno	0.89
Agglutinated spatter and clastogenic lava flows from Mavro Vouno and Kokkino Vouno	0.14
Limestones and marbles	4.84
Metapelites with metapsammites, metavolcanics and marbles	0.54
Dyke	0.05
Scree	0.51
Beach	0.70
Landslip deposits	0.10
Dacites 46–47/Palea Kammeni	0.46
Dakites 726/Palea Kammeni	0.06
Dakites 1570–1573/Nea Kammeni	0.09
Dacites 1707–1711/Nea Kammeni	0.37
Dacites 1866–1870/Nea Kammeni	1.21
Dacites 1925–1928/Nea Kammeni	0.83
Dacites 1939–1941/Nea Kammeni	0.67
Dacites 1950/Nea Kammeni	0.01
Ashes from 1925 to 1950 eruptions (over 1866 to 1870 lavas)	0.14

The above techniques were applied using Sentinel-1 Toolbox software. Finally the de-speckled image was enhanced using a histogram linear 2% stretch (Fig. 4 a).

The resulted image was imported to ArcMap where it was used as a background map in order to digitize the lineaments which represent possible tectonic lines (faults). The lineaments delineated are shown in Fig. 4 b. A number of lineaments shown on the processed ENVISAT image are not depicted in Fig. 4 b since they represent lines of drainage network or of man-made activities. Two sub-categories are indicated: (1) "lineaments-cliffs" and (2) "lineaments-other". "Lineaments-cliffs" are lineaments that can be easily verified as faults since they are located along the shoreline, mainly inside the caldera, or within the crystalline bedrock of Thera and they are featured by their sharp declination of slopes. "Lineaments-other", are mainly found within the recent pyroclastic deposits, making necessary more detailed tectonic identification in order to rank them as faults.

The rose diagrams of the faults delineated from the geological map of IGME (1980), the neotectonic map by Mountrakis et al. (1998) and the geological map of Druitt et al. (1999), together with the lineaments extracted by ENVISAT image, are depicted in Fig. 5.

By comparing the rose diagrams of faults and lineaments (Fig. 5), the following remarks can be made:

- From the rose plot of the tectonic features of the geological map of IGME (1980), two major groups of faults can be delineated, one with direction almost N-S, and another with NW-SE direction.
- From the rose plot of the tectonic features of the neotectonic map by Mountrakis et al. (1998), a major group of faults with NW-SE direction and a minor group with NE-SW direction can be distinguished.
- From the rose plot of the tectonic features of the geological map by Druitt et al. (1999), the main and only direction of the faults is NE-SW.
- From the rose-plot of the tectonic features of the lineaments delineated by the ENVISAT/ASAR radar satellite image, three groups of lineaments can be distinguished: The first one, having NW-SE direction, a second, having NE-SW direction and a third, showing almost N-S direction of azimuth values.

Field validation

The next step was to perform the necessary field-visit in order to verify the results from the digital image processing of the satellite imagery. A list of photos from Santorini islands/

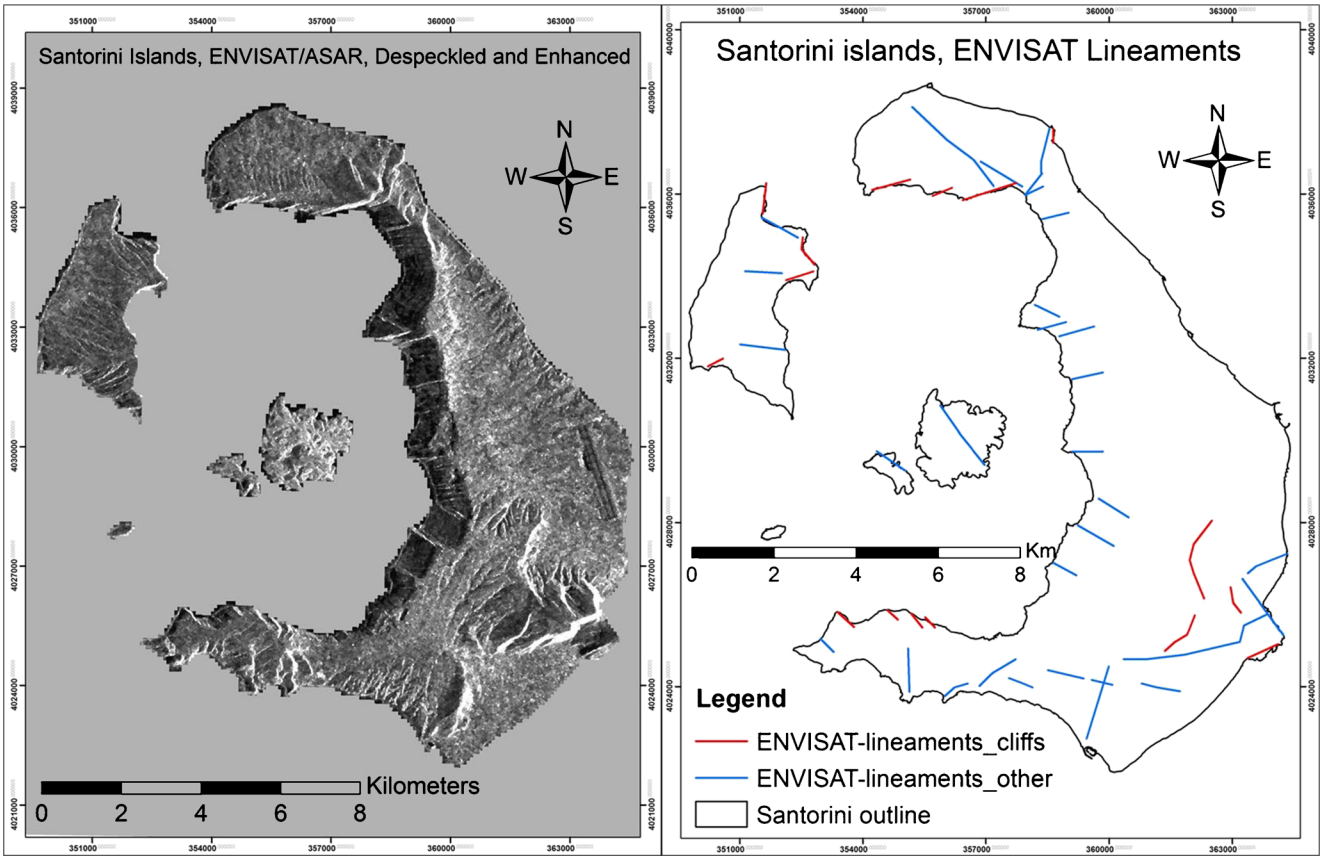

Fig. 4 **4a**/left: ENVISAT/ASAR satellite image. **4b**/right: Lineaments drawn from ENVISAT image

ground-truth visit, showing the geological structure (lithology and tectonics) at certain points, together with a map with the location of the photos, is shown in Fig. 6. In details:

6a Dacitic lavas at Nea Kammeni island from the 1866 eruption, clearly distinguished in Pleiades 1A image in "gold" colour (Fig. 3 b). The orange colour at the base is produced by iron oxides.

6b Phases 1–3, rhyodacitic pumice of the 1613 BC eruption. Megalokhorion quarry. These phases are depicted in brown-reddish colours in Fig. 3 a.

6c Lithological boundary between Phase 3 (rhyodacitic pumice) and Phase 4 (Rhyodacitic Ignimbrite) of the 1613 BC eruption. Akrotiri area. One can notice how similar these two phases appear in the field and how easily they can be distinguished in Pleiades 1A image with brown and greenish colours, respectively (Fig. 3 a).

6d Andesites and basaltic cones of the Akrotiri peninsula. The photo depicts andesitic cinder cones of Cape Mavrorachidi (the famous Red Beach).

6e Limestones and marbles. Photo from the village of Perissa (Mt. Mesa Vouno).

6f Black scoria from Mavro Vouno cinder cone.

6g A lineament verified as a fault at Mesa Vouno area.

6h A lineament verified as a fault underneath the village of Oia.

Conclusions

A geological mapping of Santorini islands was performed using Pleiades 1A satellite imagery for lithological mapping and an ENVISAT/ASAR radar satellite image for tectonic mapping (lineaments). The results were compared to the lithological units digitized from the most recent geological map and the faults from three different geological tectonic maps. Finally a ground-truth visit followed in order to verify the remote sensing findings.

Two (2) novel false colour composite Pleiades 1A satellite images, 1,4,PC4:RGB and 4,2,1:RGB proved to be the most reliable in discerning lithological units. On the other hand, a properly de-speckled (refined Lee filter) ENVISAT/ASAR radar image, produced the best results in delineating lineaments, which are presumable faults.

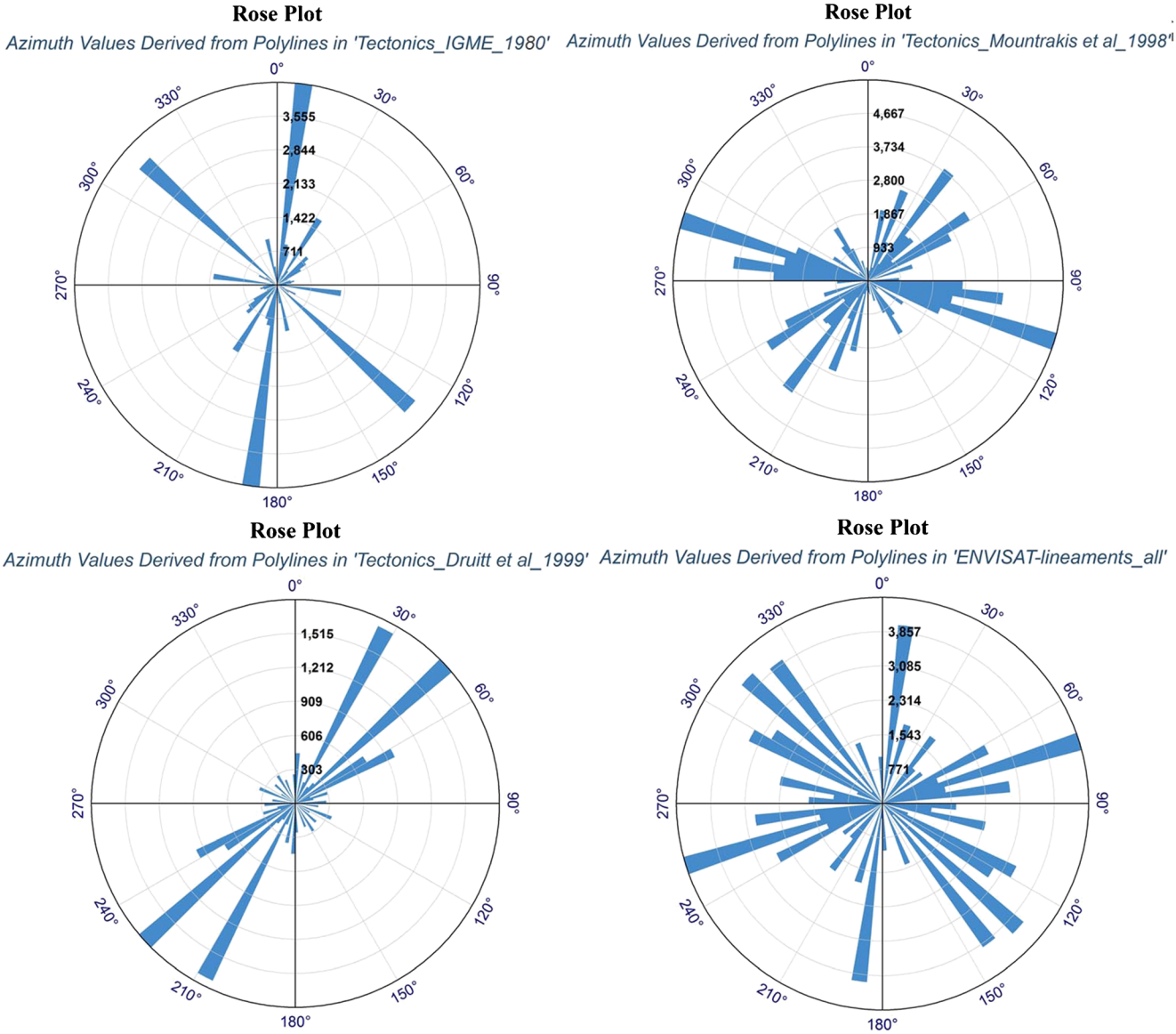

Fig. 5 Rose diagrams of the tectonics derived by various geological maps and of lineaments derived by ENVISAT/ASAR radar image

Considering lithological units mapped on the geological map and on the satellite imagery, the geological map proved to be reliable in most of the cases with two exceptions found:

6i On the island Nea Kammeni, where a thin ash layer over the 1866–1870 lavas was detected using satellite images (Fig. 3 b). This layer was created by the volcanic eruptions of 1925–1928, 1939–1941 and 1950

- On the southern part of Thera island, the lithological unit "Phases 1–3, Rhyodacitic Pumice", seems to cover a more extended area than the area that is depicted on the geological map (Figs. 2b and 3) covered by "Phase 4, Rhyodacitic Ignimbrite" on the geological map.

The colour distinction between Phases 1–3 and Phase 4 of the 1613 ± 13 BC eruption on the Pleiades satellite imagery proved to be a relatively easy task at the southern part of Thera island, less easy at the eastern part and finally, turning gradually to a difficult task at the northern part of Thera and in Therasia island, where Phase 4 is depicted with very similar colours to Phases 1–3. The explanation to this differentiation comes from Druitt (2014), where he explains that Phase 4 in the last case is rich in lithic blocks, like underlying Phase 3 of the eruption, because "it was fed by pyroclastic flows that were funneled through the NW breach of the caldera".

Fig. 6 Photographs of the ground-truth visit in various areas of Santorini island complex, verifying the presence of certain rocks and lineaments detected on the satellite imagery ▶

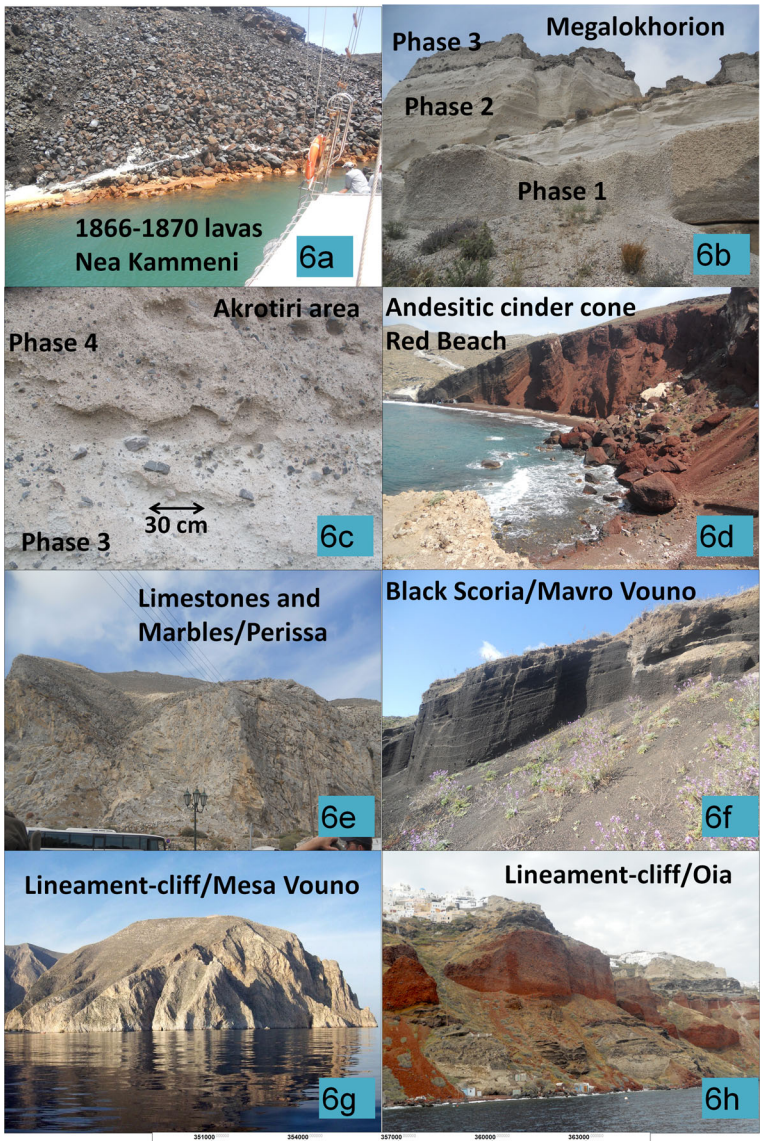
1866-1870 lavas
Nea Kammeni
6a
Phase 3
Megalokhorion
Phase 2
Phase 1
6b
Akrotiri area
Phase 4
30 cm
Phase 3
6c
Andesitic cinder cone
Red Beach
6d
Limestones and
Marbles/Perissa
6e
Black Scoria/Mavro Vouno
6f
Lineament-cliff/Mesa Vouno
6g
Lineament-cliff/Oia
6h
Santorini islands, points of photos
N
W
E
S
6f
6h
6a
6b
6c
6d
6e
6g
Km
0 2 4 6 8

The differences in the lithology drawn from the geological map and Pleiades 1A images are limited in two areas of the island complex. This fact does not lessen the importance of the methodology, but rather raises it, since despite the detailed geological mapping of the famous volcano, new findings were verified that will enable geoscientists to improve the existing geological maps.

The conclusion that can be extracted from the comparison of the rose plots of faults and lineaments (Fig. 5), is that the lineaments drawn from the satellite image, include all major directions of azimuth values, drawn on the three other geological-neotectonic maps, underlining thus the persuasion that it stands as a valuable and trustworthy methodology for extracting tectonic features. Furthermore, the ground-truth visit into areas of "lineaments-cliffs" (Fig. 6 g, h) showed clearly from their geomorphologic appearance that they testify as faults. It is necessary of course that a more thorough study of the whole number of lineaments follows, taking into consideration specialized tectonic indices and measurements.

As a final conclusion, the geological map of Santorini island complex needs minor revision concerning lithological boundaries, in order to include the new findings derived by the satellite imagery, as they were verified by ground-truth visit. The lineaments' findings from the satellite images have been so-far validated, and they will contribute to the revision of tectonic lines when completed. The methodology followed in this study can be of great value since it produces reliable results that can be applied on other study areas in Greece or elsewhere, where suchlike data are available to the researchers, provided that similar climatic and vegetation-cover conditions prevail.

Acknowledgements The Pleiades 1A satellite images were kindly provided by Airbus Defence and Space (ordered via Geostore), through ESA's Category-1 Project ID:29826 and the ENVISAT/ASAR image was provided by ESA through the framework of the same Project.

References

Arlegui LE, Soriano MA (2003) An example of a comparison between Thematic Mapper and radar images in the central Ebro basin. Int J Remote Sens 24(3):457–474

Behnia P, Harris JR, Rainbird RH, Williamson MC, Sheshpari M (2012) Remote predictive mapping of bedrock geology using image classification of Landsat and SPOT data, western Minto Inlier, Victoria Island, Northwest Territories, Canada. Int J Remote Sens 33(21): 6876–6903

Bogdanov I, Huaman D, Thovert JF, Genthon P, Adler PM (2011) Tectonic stresses seaward of an aseismic ridge—Trench collision zone. A remote sensing approach on the Loyalty Islands, SW Pacific. Tectonophysics 499:77–91

Druitt TH (2014) New insights into the initiation and venting of the Bronge-Age eruption of Santorini (Greece), from componenet analysis. Bull Volcanol 76:794

Druitt TH, Edwards L, Mellors M, Pyle DM, Sparks RSJ, Lanphere M, Davies M, Barriero B (1999) Santorini Volcano (Geological map of the Santorini islands, Scale 1/20.000). Geological Society Memoir No. 19, London.

European Space Agency/ESA (2005) Spaceborne radar applications in Geology (ESA TM-17). ESA Publications Division, ESTEC, Noordwijk

Friedrich WL, Kromer B, Heinemeier J, Friedrich M, Pfeiffer T, Talamo S (2006) Santorini eruption radiocarbon dated to 1627–1600 B.C. Science 312(5773):548Apr 28

Hadigheh SMH, Ranjbar H (2013) Lithological mapping in the eastern part of the Central Iranian Volcanic Belt using combined ASTER and IRS data. J Indian Soc Remote Sens 41(4):921–931

He J, Harris JR, Sawada M, Behnia P (2015) A comparison of classification algorithms using Landsat-7 and Landsat-8 data for mapping lithology in Canada's Arctic. Int J Remote Sens 36(8):2252–2276

Institute of Geology and Mineral Exploration/IGME (1980) Geological map of 1/50.000 scale. Sheet: Thira island.

Jakob S, Bühler B, Gloaguen R, Breitkreuz C, Eliwa HA, Gameel KE (2015) Remote sensing based improvement of the geological map of the Neoproterozoic Ras Gharib segment in the Eastern Desert (NE-Egypt) using texture features. J Afr Earth Sci 111:138–147

Liu B, Jiang W, Zhang J, Luo Y, Gong L (2010) Wenchuan earthquake ruptures located by offset-tracking procedure of ENVISAT ASAR amplitude images. Earthq Sci 23:283–287

Morelli M, Piana F (2006) Comparison between remote sensed lineaments and geological structures in intensively cultivated hills (Monferrato and Langhe domains, NW Italy). Int J Remote Sens 27(20):4471–4493

Mountrakis D, Pavlides S, Chatzipetros A, Meletlidis S, Tranos M, Vougioukalakis G, Kilias A (1998) Active deformation of Santorini. In Proceedings of the second workshop Santorini, Greece, 2–4 May 1996:13–22.

O'Leary DW, Friedman JD, Pohn HA (1976) Lineament, linear, lineation: some proposed new standards for old terms. Bull Geol Soc Am 87:1463–1469

Othman AA, Gloaguen R (2014) Improving lithological mapping by SVM classification of spectral and morphological features: the discovery of a new chromite body in the Mawat ophiolite complex (Kurdistan, NE Iraq). Remote Sens 6:6867–6896

Pal SK, Majumdar TJ, Bhattacharya AK (2007) Usage of ERS SAR data over the Singhbhum shear zone, India for structural mapping and tectonic studies. Geocarto Int 22(4):285–295

Pour AB, Hashim M (2015a) Evaluation of Earth Observing-1 (EO1) data for lithological and hydrothermal alteration mapping: a case study from Urumieh-Dokhtar Volcanic Belt, SE Iran. J Indian Soc Remote Sens 43(3):583–597

Pour AB, Hashim M (2015b) Structural mapping using PALSAR data in the Central Gold Belt, Peninsular Malaysia. Ore Geol Rev 64:13–22

Pournamdari M, Hashim M, Pour AB (2014) Spectral transformation of ASTER and Landsat TM bands for lithological mapping of Soghan ophiolite complex, south Iran. Adv Space Res 54:694–709

Prieto EF, Quénéhervé G, Bachofer F, Shahzad F, Maerker M (2015) Morphotectonic interpretation of the Makuyuni catchment in Northern Tanzania using DEM and SAR data. Geomorphology 248:427–439

Rowan LC, Mars JC (2003) Lithologic mapping in the Mountain Pass, California area using advanced spaceborne thermal emission and reflection radiometer (ASTER) data. Remote Sens Environ 84:350–366

Saadi NM, Watanabe K (2009) Assessing image processing techniques for geological mapping: a case study in Eljufra, Libya. Geocarto Int 24(3):241–253

Yamaguchi Y, Naito C (2009) Spectral indices for lithologic discrimination and mapping by using the ASTER SWIR bands. Int J Remote Sens 24(22):4311–4323

Zhang X, Li P (2014) Lithological mapping from hyperspectral data by improved use of spectral angle mapper. Int J Appl Earth Obs Geoinf 31:95–109